J Wood Sci (2011) 57:107–113
DOI 10.1007/s10086-010-1148-8

ORIGINAL ARTICLE

Pierre Berard · Ping Yang · Hidefumi Yamauchi
Kenji Umemura · Shuichi Kawai

Modeling of a cylindrical laminated veneer lumber II: a nonlinear finite element model to improve the quality of the butt joint

Received: February 5, 2010 / Accepted: July 26, 2010 / Published online: February 26, 2011

Abstract The use of low-grade logs to build spirally wound laminated veneer lumber (LVL) has been studied and improved from the point of view of the gluing process, fiber orientation angle, and end joint of the LVL. The butt joint appears to be the fracture point when the column is submitted to a compressive or bending load. Owing to the complexity of cylindrical LVL, we used a finite element method to simulate the mechanical behavior of part of its wall. This part was small enough to be considered flat but was representative of the structure, especially in the area of the butt joint. This allowed us to test the validity of different settings of the parameters involved in the manufacturing process. To feed data for this model, we used the results established for the linear and nonlinear behavior of raw hinoki in Part I of this series of articles. We then used this numerical model to improve the quality of the butt joint by testing different settings of the joint. We show that reducing the butt joint gap under 0.5 mm, which requires only a few changes in the production line, provides an important increase in the modulus of rupture and nonnegligible improvement of the modulus of elasticity compared to that for a ≥ 1 mm butt joint gap.

Key words Cylindrical LVL · Butt joint · Finite elements method

P. Berard (✉) · K. Umemura · S. Kawai
Research Institute for Sustainable Humanosphere, Kyoto University, Gokasho, Uji, Kyoto 611-0011, Japan
Tel. +81-774-38-3670; Fax +81-774-38-3678
e-mail: berard.pierre@gmail.com

P. Yang
Department of Technology Education, Faculty of Education, Kumamoto University, Kumamoto 860-8555, Japan

H. Yamauchi
Institute of Wood Technology, Akita Prefectural University, Noshiro 016-0876, Japan

Parts of this paper were presented at the 56th Annual Meeting of the Japan Wood Research Society, Akita, Japan (2006)

Introduction

Cylindrical laminated veneer lumber (LVL) (Fig. 1) is a biomimetic structural product comprised of several plies of veneer helically wound along a steel mandrel. After winding a high-grade veneer on the external side of the LVL, a rubber belt or an airbag is applied on the periphery of the LVL. Sufficient tension or pressure to cure the product is then applied before the steel mandrel is removed.

Many studies have been performed on this product that have covered a wide range of topics and problems involved in its production. Some mechanical properties of the LVL have been investigated, depending on the species and the number of layers. Yamauchi et al.[1] showed that the four-point bending modulus of elasticity (MOE) is not particularly influenced by the number of the plies over six plies (it varies from 8.72 GPa for 6 plies to 8.73 GPa for 10 plies). On the other hand, in the same range of number of plies, the modulus of rupture (MOR) was found to vary between 8.84 MPa (6 plies) and 14.81 MPa (10 plies) because of the existence of a gap through the layers where the interlocked layers meet (cross-sectional gap). The impact of the angle of the interlocked plies has been studied as well[2] using a theoretical method of homogenization; the study showed a rapidly decreasing MOE with an increasing angle. According to the results of the study, an angle of 10° has been accepted as a good compromise between production needs and the required MOE. There have also been several numerical analyses of the end of the column, where it connects with other structural members. An interest in a round glulam core inserted at the end of the column has been established[3] using the finite element model (FEM), and different fillers of the column for improving strength and connectivity with other members have been explored.[4]

Several gluing techniques were tried – such as the use of a combination of urea-formaldehyde resin with isocyanate resin and a combination of resorcinol meta-aminophenol with ordinary resorcinol resin – to improve the efficiency of the production.[5] Various ways to apply the resins have been evaluated as well, such as the use of paper rolls as vectors

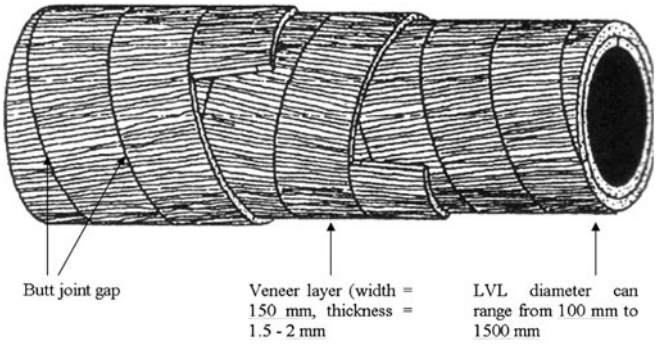

Fig. 1. Schema for cylindrical laminated veneer lumber (LVL)

Table 1. Settings for flat laminated veneer lumber

Layer	Angle (°)	Shift (mm)
1	10	0
2	–10	0
3	10	75
4	–10	75
5	10	0
6	–10	0
7	10	75
8	–10	75
9	10	0
10	–10	0

of the glue line.[6] In the same field, an improved spiral winder has been designed[7] and successfully tested; it includes a heating device to reduce the curing time and allow the use of a continuous rubber band to apply pressure.

However, the butt joint remains a weak point when the column is submitted to compression or bending. Taking this into consideration as well as the difficulty to produce cylindrical LVLs with a variety of settings for experimental purposes, we decided to study the impact of the butt joint gap and fiber angle via an FEM and then to determine whether the new settings that would be required on the production line are worth it.

A former study showed that the mechanical characteristics of a flat sample can be related to those of a cylindrical one.[8] An FEM was then written using MSC.MARC MENTAT finite elements software. This model represents a small part of the cylinder wall that is assumed to be flat because of its dimensions in width compared to the effective diameter of a cylindrical LVL. In the axial direction of the LVL, the FEM is long enough to be representative of the structure.

The first point then was to model a 10-ply interlocked flat LVL sample and compare its behavior during bending with that of a series of samples presenting the same characteristics made of rotary peeled veneers of hinoki (Japanese cypress, or *Chamaecyparis obtusa*). We thus showed that the linear and nonlinear mechanical properties established in Part I of this series of articles, combined with an FEM of a four-point bending test, allows us to describe with accuracy the behavior of the real flat LVL in terms of the MOE and MOR. Regarding the MOR, we discussed the failure criteria[9] to give a result closest to that of the experimental result. Then, the relations between the butt joint gap and the MOE and MOR were investigated in regard to different fiber angles.

Materials and methods

Raw material

The raw material used for experiments consists in three hinoki trees grown in the Yoshino area, Nara Prefecture, Japan. They were 80–100 years old at the time of harvesting, with a diameter of around 30 cm at breast height. After harvesting, three 1.3-m logs were cut from each tree beginning at the bottom. Six of these nine logs (L_1–L_6), stored in water, were peeled for veneer. The three remaining logs (L_7–L_9), stored in air conditioning, were cut into samples for the experiments described in the Part I article.

Bending four-point flat LVL samples

We first prepared a panel made of 10 layers of peeled veneers obtained by peeling logs L_1–L_6. After peeling, the veneers were stored in a controlled-environment room [20°C, 65% relative humidity (RH)] to let them dry to 14.50% moisture content (MC). The dimensions of this panel were 800 × 800 mm. The veneers were 2 mm thick in the radial (R) direction, 150 mm wide in the parallel to the grain (L) direction, and around 1 m long in the tangent (T) direction. Table 1 describes the setting of each layer in terms of the angle and shifting along the main axis of the board.

The LVL comprises 10 interlocked (± 10°) plies, each ply being composed of 150 mm wide veneer plies (Fig. 2). Between each ply there is a butt joint. Every "+10°" ply is shifted ± 75 mm, regarding the other "+10°" plies, and so on, with the "–10°" plies. We used resorcinol formaldehyde adhesive, which was manually sprayed to an amount of 280–300 g/m^2 using a hand roller. During the setting of the veneers, we took great care to maintain the butt joint gap as reduced as possible.

After setting, the panel was placed under a hydraulic press equipped with heating plates set at 60°C. The panel was then pressed at 0.3 MPa for 3 h. After curing, the panel was stored in a controlled-environment room (20°C, 65% RH) for 3 weeks.

Ten flat LVL samples were cut in the panel, their dimensions being 19.5 mm (R direction) × 20 mm (T direction) × 400 mm (L direction). The 10 samples were then tested using a four-point bending bench on a 4411 Instron machine (Norwood, MA, USA) equipped with a 5-kN load cell, according to the specifications of the NF-EN-408 French Standard[10] for LVL testing.

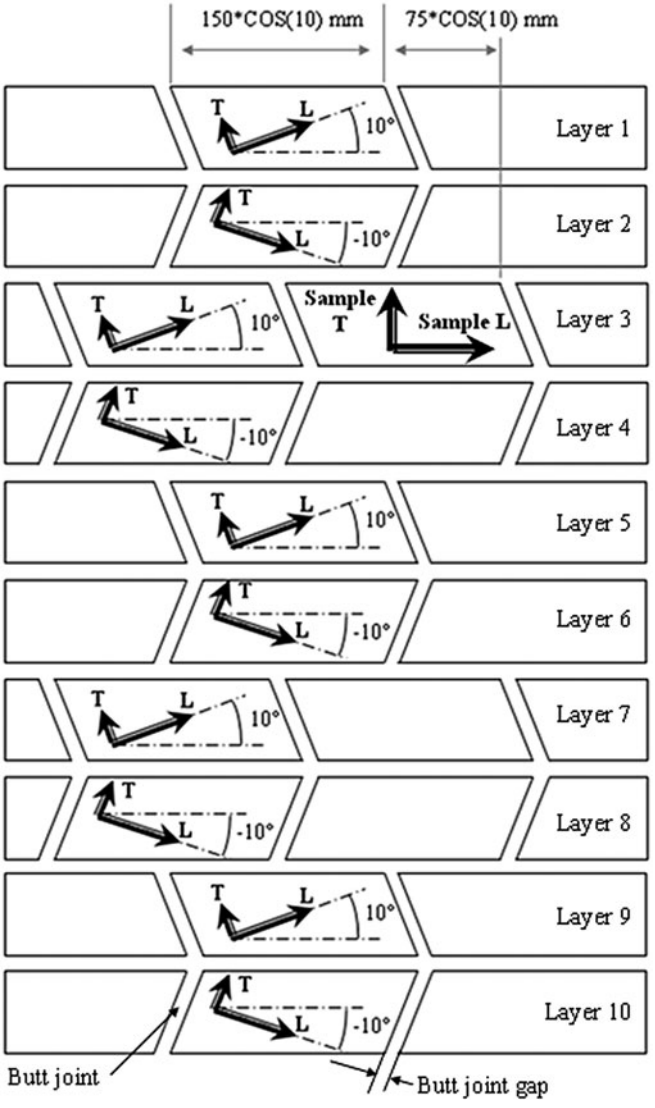

Fig. 2. Setting of the first 10 layers of flat LVL. *T*, tangential direction; *L*, parallel to the grain direction

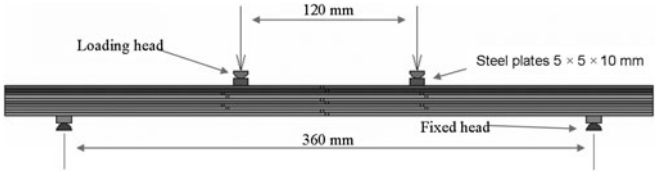

Fig. 3. Four-point bending finite element method (FEM) model

Settings for the FEM of a four-point bending test of 10-layer flat LVL

The FEM software used was MSC.MARC MENTAT 2005. The model (Fig. 3) had a butt joint gap of 0.5 mm. This value constitutes an average of what we observed on the flat LVL samples used to prepare the experimental samples after cutting and measuring them. Some of those gaps are totally or partially filled with glue, which is not taken into account in the FEM model. The layers of the model were also set to a thickness of 1.95 mm to match the final dimensions of the samples after pressing and curing.

The finite elements used were eight nodes quadrilaterally, the meshing being affected by a bias factor that allowed refining the mesh in the areas of the butt joint. We used exactly the same settings as those of the FEM for raw hinoki (see the Part I article). The first yield stress ratio was set to 0.855, as the experimental first yield stress during bending was established at 21.55 MPa for raw hinoki.

We compared three criteria to detect failure: the Tsai-Wu criterion, the Hoffman criterion, and the maximum stress criterion. Those criteria require that we know the strengths in both the compression and tensile directions as well as the shear strength. Each criterion calculates, at each point of integration, the value of the F index. When this index reaches 100%, failure is said to appear.

The Tsai-Wu criterion is as follows

$$F = \begin{bmatrix} D_1\sigma_R + D_2\sigma_T + D_3\sigma_L + D_4\sigma_R^2 + D_5\sigma_T^2 + D_6\sigma_L^2 \\ + \dfrac{\sigma_{RT}^2}{\sigma_{RTmax}^2} + \dfrac{\sigma_{TL}^2}{\sigma_{TLmax}^2} + \dfrac{\sigma_{RL}^2}{\sigma_{RLmax}^2} + 2F_{12}\sigma_R\sigma_T \\ + 2F_{23}\sigma_T\sigma_L + 2F_{13}\sigma_R\sigma_L \end{bmatrix} \quad (1)$$

$$D_1 = \left(\frac{1}{\sigma_{R-t}} - \frac{1}{\sigma_{R-c}}\right) \quad D_4 = \left(\frac{1}{\sigma_{R-t}\times\sigma_{R-c}}\right)$$

$$D_2 = \left(\frac{1}{\sigma_{T-t}} - \frac{1}{\sigma_{T-c}}\right) \quad D_5 = \left(\frac{1}{\sigma_{T-t}\times\sigma_{T-c}}\right)$$

$$D_3 = \left(\frac{1}{\sigma_{T-t}} - \frac{1}{\sigma_{T-c}}\right) \quad D_6 = \left(\frac{1}{\sigma_{T-t}\times\sigma_{T-c}}\right)$$

where $\sigma_{x\text{-}t}$ and $\sigma_{x\text{-}c}$ are, respectively, the maximum allowable stress in the X direction in tension and in compression; σ_R, σ_T, σ_L are, respectively, the current stress in the R, T, and L directions; σ_{RTmax}, σ_{TLmax}, σ_{RLmax} are, respectively, the maximum allowable shear stress in the RT, TL, and RL planes; σ_{RT}, σ_{TL}, σ_{RL} are, respectively, the current shear stress in the RT, TL, and RL planes; and F_{RT}^2, F_{TL}^2, F_{RL}^2 are designed as interactive strength constants for, respectively, the RT, TL, and RL planes.

$$F_{RT}^2 \le \frac{1}{2}\left(\frac{1}{\sigma_{R-t}\sigma_{R-c}}\times\frac{1}{\sigma_{T-t}\sigma_{T-c}}\right)$$

$$F_{TL}^2 \le \frac{1}{2}\left(\frac{1}{\sigma_{L-t}\sigma_{L-c}}\times\frac{1}{\sigma_{T-t}\sigma_{T-c}}\right)$$

$$F_{RL}^2 \le \frac{1}{2}\left(\frac{1}{\sigma_{R-t}\sigma_{R-c}}\times\frac{1}{\sigma_{L-t}\sigma_{L-c}}\right)$$

The Hoffman criterion is as follows

$$F = \begin{bmatrix} C_1(\sigma_T - \sigma_L)^2 + C_2(\sigma_L - \sigma_R)^2 \\ + C_3(\sigma_R - \sigma_T)^2 + C_4\sigma_R + C_5\sigma_T \\ + C_6\sigma_L + C_7\sigma_{TL}^2 + C_8\sigma_{RL}^2 + C_9\sigma_{RT}^2 \end{bmatrix} \quad (2)$$

$$C_1 = \frac{1}{2}\left(\frac{1}{\sigma_{L-t}\sigma_{L-c}} + \frac{1}{\sigma_{T-t}\sigma_{T-c}} - \frac{1}{\sigma_{R-t}\sigma_{R-c}}\right)$$

$$C_2 = \frac{1}{2}\left(\frac{1}{\sigma_{R-t}\sigma_{R-c}} + \frac{1}{\sigma_{L-t}\sigma_{L-c}} - \frac{1}{\sigma_{T-t}\sigma_{T-c}}\right)$$

$$C_3 = \frac{1}{2}\left(\frac{1}{\sigma_{R-t}\sigma_{R-c}} + \frac{1}{\sigma_{T-t}\sigma_{T-c}} - \frac{1}{\sigma_{L-t}\sigma_{L-c}}\right)$$

$$C_4 = \frac{1}{2}\left(\frac{1}{\sigma_{R-t}} + \frac{1}{\sigma_{R-c}}\right)$$

$$C_5 = \frac{1}{2}\left(\frac{1}{\sigma_{T-t}} + \frac{1}{\sigma_{T-c}}\right)$$

$$C_6 = \frac{1}{2}\left(\frac{1}{\sigma_{L-t}} + \frac{1}{\sigma_{L-c}}\right)$$

$$C_7 = \frac{1}{S_{TL}^2}$$

$$C_8 = \frac{1}{S_{RL}^2}$$

$$C_9 = \frac{1}{S_{RT}^2}$$

where σ_R, σ_T, σ_L, σ_{RT}, σ_{TL}, σ_{RL}, $\sigma_{x\text{-}t}$, and $\sigma_{x\text{-}c}$ (X being R, T, or L) are defined the same as in the case of the Tsai-Wu criterion. In addition, S_{RT}, S_{TL}, S_{RL} are the maximum allowable in-plane shear stresses.

The maximum stress criterion is as follows (it consists in six expressions that are calculated at each point of integration)

$$\left[\begin{array}{l}\left(\frac{\sigma_R}{X_t}\right)\Big/F \quad \text{if} \quad \sigma_R > 0 \\ \left(-\frac{\sigma_R}{X_c}\right)\Big/F \quad \text{if} \quad \sigma_R < 0\end{array}\right] \tag{3}$$

$$\left[\begin{array}{l}\left(\frac{\sigma_T}{Y_t}\right)\Big/F \quad \text{if} \quad \sigma_T > 0 \\ \left(-\frac{\sigma_T}{Y_c}\right)\Big/F \quad \text{if} \quad \sigma_T < 0\end{array}\right] \tag{4}$$

$$\left[\begin{array}{l}\left(\frac{\sigma_L}{Z_t}\right)\Big/F \quad \text{if} \quad \sigma_L > 0 \\ \left(-\frac{\sigma_L}{Z_c}\right)\Big/F \quad \text{if} \quad \sigma_L < 0\end{array}\right] \tag{5}$$

$$\left(\left|\frac{\sigma_{RT}}{S_{RT}}\right|\right)\Big/F \tag{6}$$

$$\left(\left|\frac{\sigma_{TL}}{S_{TL}}\right|\right)\Big/F \tag{7}$$

$$\left(\left|\frac{\sigma_{RL}}{S_{RL}}\right|\right)\Big/F \tag{8}$$

where X_t and X_c are the maximum stresses in the 1-direction in tension and compression, respectively; Y_t and Y_c in the 2-direction; and Z_t, Z_c in the 3-direction. σ_R, σ_T, σ_L, σ_{RT}, σ_{TL}, σ_{RL}, S_{RT}, S_{TL}, S_{RL} are defined the same as for the Tsai-Wu criterion.

FEM model 2 to improve the quality of the butt joint

The aim of this part of the article is to study the relations existing between the butt joint gap and the MOE and MOR as well as the gain in terms of stiffness and strength we can expect by reducing the butt joint. We also checked the impact of the fiber angle on the MOE and MOR.

This FEM was set up in the form of a bending four-point sample using a fully parametric design to be able to test different settings of the butt joint gap of the sample. We used exactly the same settings, plastic model, failure criteria, and material properties as those of the FEM for the raw hinoki (see the Part I article). The model is made of 10 interlocked layers of hinoki, set up as described in Fig. 4. The width of the central layer was set to 150 mm, as was the case for the samples used for the experiments. The outer layers were set up to make the sample length equal to 400 mm. The FEM was set with the material properties of the hinoki, as determined in the Part I article.

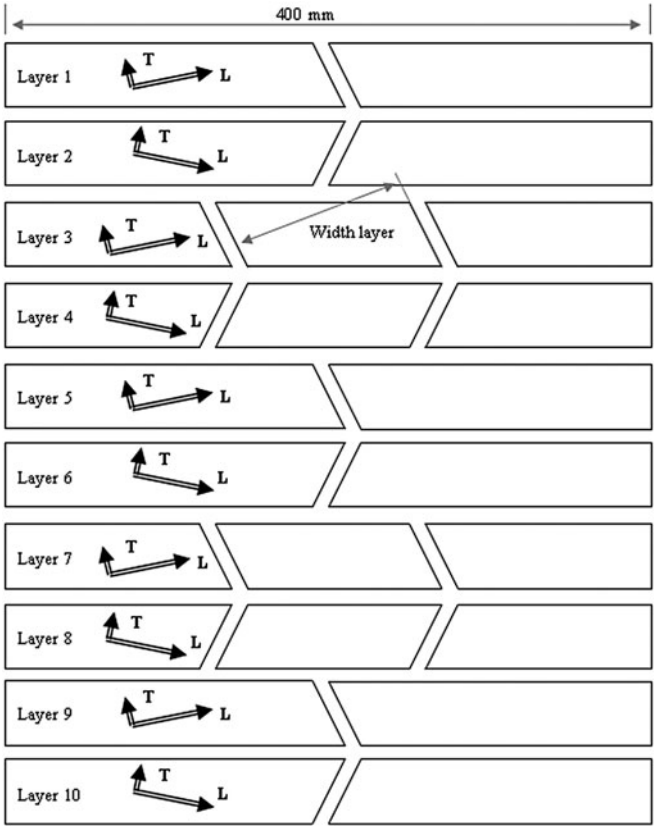

Fig. 4. Settings of the first four layers of the flat LVL model to improve no. 2

Results and discussion

Experimental bending test of 10-ply flat LVL

Following the recommendations of the NF-EN-408 French Standard.[10] the bending MOE reached 8.6 GPa [2.5% standard deviation SD)]. The mean MOR was established at 47.1 MPa (8.1%) for a mean deflection of 11.06 mm (11.5%).

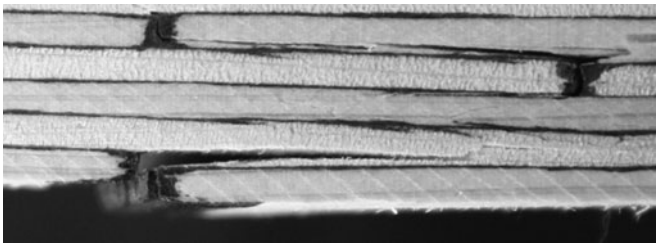

Fig. 5. Typical rupture of a bending four-point flat LVL sample occurring in the ninth layer, under the butt joint of the tenth layer (tension side)

Table 2. MOR calculated using various failure criteria

Criterion	MOR according to the criterion (MPa)	Variation regarding experimental MOR (= 47.1 MPa) (%)
Tsai Wu	36.3	23.1
Hoffman	40.8	13.4
Maximum stress	38.5	18.4

MOR, modulus of rupture

FEM model of a four-point bending test of 10-ply flat LVL

The bending MOE established at 9.2 GPa (compared to 8.6 GPa in the experimental test). The stress corresponding to a deflection of 11.06 mm is equal to 42.7 MPa, which means a variation of 9.3% regarding the experimental MOR. Those values show the accuracy of the FEM model when describing the elastic and nonlinear behavior of the flat LVL. Regarding the prediction of failure, we set the model to display the failure criterion indexes along a "path plot" placed along the tension side of the ninth layer, on the tension side of the sample. This allowed us to get rid of the artifacts constituted by some nodes placed on corners of the outer layer of the veneer. Moreover, the experiments showed that fracture always starts from the ninth layer, just under the butt joint of the tenth layer (Fig. 5). The results are shown in the Table 2.

Although they are quite close to each other, these results tend to show that the Hoffman criterion is the one that gives the closest answer compared to the experimental results. It must be mentioned that the three criteria underestimate the experimental MOR, which ensures a comfortable security margin when it is used for dimensioning structures. Based on those results, we checked only the Hoffman criterion for the analysis of the relations between the butt joint gap and the MOR and MOE.

Figure 6 shows a comparison of the force–displacement curves of the experimental bending tests and the FEM bending curve. Note that the curves are close, including in the viscoplastic area.

Influence of the fiber angle on the MOE and MOR for variously sized butt joint gaps

Fig. 7 shows the evolution of the MOE as a function of the fiber angle, for the following dimensions of the butt joint gap: 0.25, 0.5, 1.0, 1.5, and 2.0 mm. The main tendency is a regular decrease in the MOE for all the gaps as the fiber angle increases, as already established by Yamauchi et al.[1] We can basically observe two sets of curves: those corresponding to butt joint gaps of 0.25 mm and 0.5 mm and those established for gaps of ≥1.0 mm.

The points corresponding to the 0.25- and 0.5-mm gaps are close, except with a 6° fiber angle in the 0.5-mm gap curve. If we exclude this point, a clear tendency can be established, as shown on Fig. 8. Concerning the 1.0-, 1.5-, and 2.0-mm gaps, it is only with a fiber angle >9.5° that a good fitting line can be determined, with some points of the

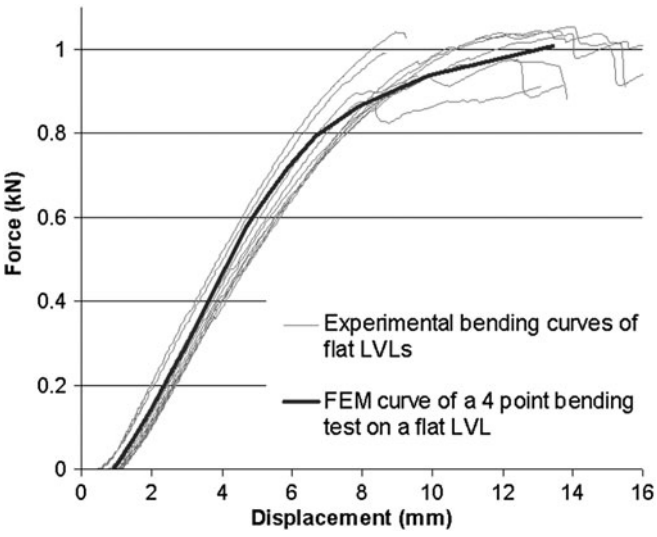

Fig. 6. Experimental and FEM models of four-point bending test curves

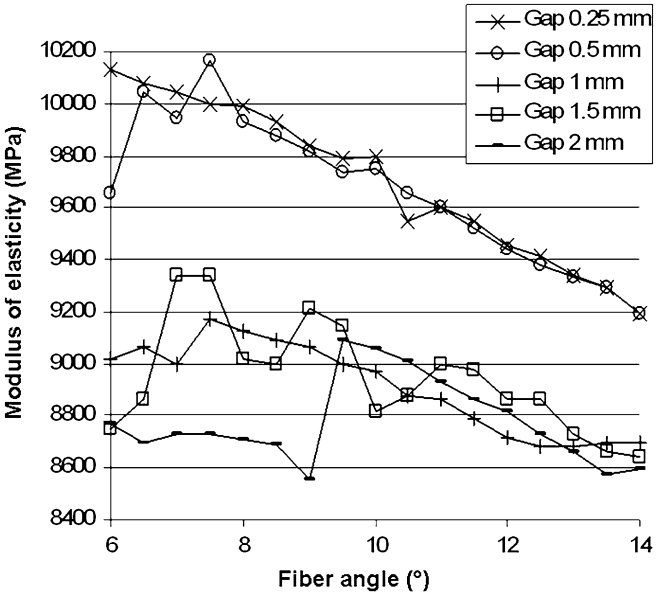

Fig. 7. Variations in the modulus of elasticity (MOE) regarding function of the fiber angle for different dimensions of the butt joint gap

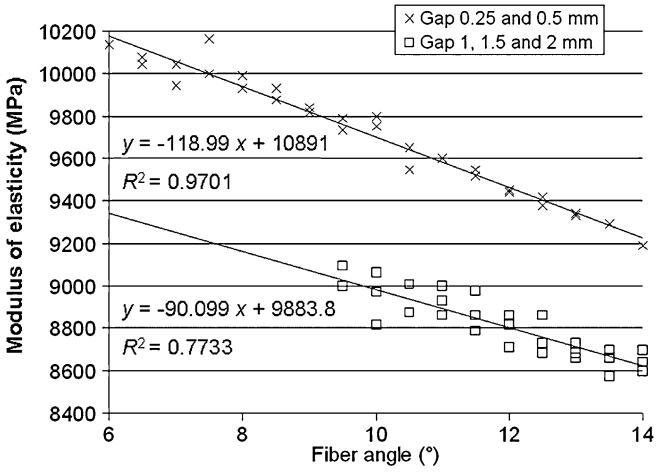

Fig. 8. Variations in the MOE regarding function of the fiber angle for different dimensions of the butt joint gap and correlation with the fiber angle

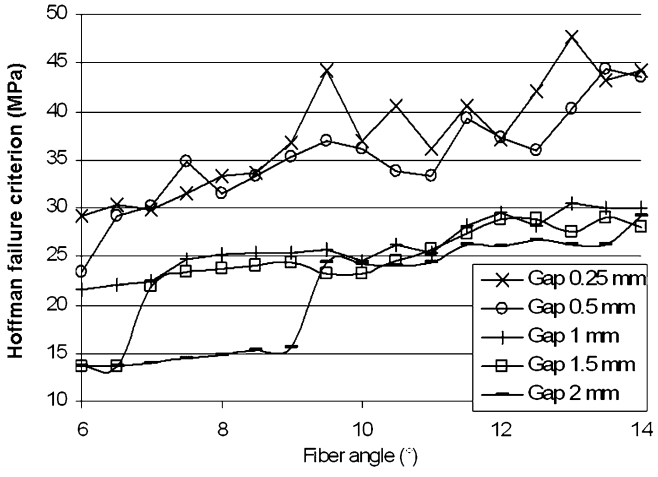

Fig. 9. Variation in the modulus of rupture (MOR) according to the Hoffman criterion regarding function of the fiber angle for different dimensions of the butt joint gap

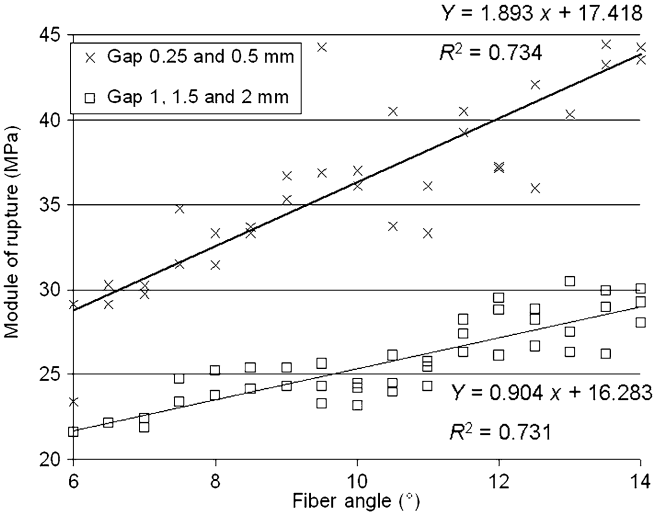

Fig. 10. Variation in the MOR regarding function of the fiber angle for different dimensions of the butt joint gap and correlation with the fiber angle

2.0-mm gap curve, mainly, disagreeing with the general tendency.

The mean difference in terms of stiffness between the two sets of values is 670.5 MPa (SD 17.6%), which represents 7.6% of the mean value of the lower set (mean MOE of the 1.0-, 1.5-, and 2.0-mm gaps for fiber angles >9° was 8818 MPa, SD 1.7%).

In the case of variations in the MOR, the curves present an inverse tendency (Fig. 9) to that of the MOE, showing for all gaps a slight increase in the MOR as the fiber angle increases. As we observed in the case of the MOE, the curves can also be separated into two sets, one for the gaps of 0.25 and 0.5 mm and another for the gaps ≥2.0 mm. The mean difference between the two distinguishable sets of values is 12.5 MPa, which represents 52.5% of the mean value of the lower set (= 23.8 MPa for butt joint gaps equal to 1.0-, 1.5-, and 2.0-mm). If we exclude some points for the lower angle values (<9° for the 1.5- and 2.0-mm butt joint gaps curves), good tendencies can be established (Fig. 10) as well as for the MOE, showing that globally the MOR is also well correlated with the fiber angle, regardless of the size of the butt joint gap.

Thus, both MOE and MOR are well correlated with the fiber angle, and this observation is not dependent on the butt joint gap. The points that have to be excluded for the smaller fiber angles in the case of the 1.5- and 2.0-mm curves are supposedly artifacts.

The sudden increase in the MOE and especially the MOR between 0.5 mm and 1.0 mm results from the fact that in that case the two ends of the layers facing each other in the butt joint come into contact while the material is not yet damaged. Because the glue line is very stiff, the impact on the MOE is not high, as we noted (+7.6 MPa); the increase corresponds to the reduced size of the cross joint and, consequently, the size of the defect in the structure. The influence on the MOR is greater because with this additional contact between layers the compressed side of the specimen is reinforced in the area of the butt joint, reducing its deflection for a given load, compared to butt joint gaps of greater dimension. This contact artificially reinforces the structure, starting from a given deflection. When this occurs at a time when the material is not already damaged (i.e., early after the first yield point), it produces an important increase in strength during bending.

In the case of the MOR, the relation can be extended not only to the butt joint gap but to the contact surface that depends directly on the butt joint gap value (Fig. 11) centered at the crossing of two superposed butt joints. This contact surface (cross-hatched area in Fig. 11) is the only physical link between the layers as two layers of veneer are glued at each other only there. The surface of this area is directly related to the fiber angle and the joint gap value: the smaller the gap, the higher the angle, the wider the

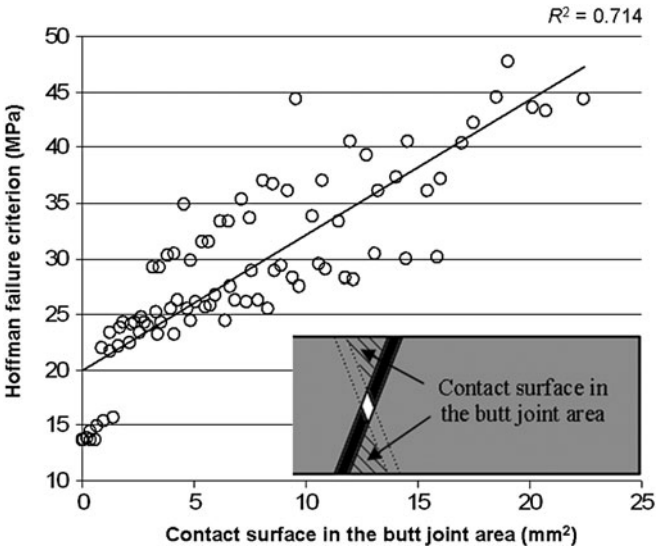

Fig. 11. Relation between the MOR and the contact surface in the butt joint area: details of the contact surface

surface. Figure 11 shows that the MOR is directly related to the surface of the contact area under the butt joint.

This lets us assume that the compressive strength is reinforced by a reduction in the butt joint gap; but in a progressive manner, resistance should increase as the contact surface increases. This is one of the future goals of the studies related to cylindrical LVL, which requires collection of other experimental data to determine if the FEM described here can provide accurate results when applied to compression.

Conclusion

This article described results obtained by different scales. First, generally speaking, we showed that it is possible to predict the behavior of complex composites made of biological components using the FEM. Such a numerical approach, although requiring experimental data collection on the raw materials concerned, allows us to avoid heavy experimental work on the influence of parameters when talking of composite structures. This is an effective, sustainable way to study complex problems with multiple parameters.

In particular, we compared stress–strain curves derived from experimental four-point bending tests and those from an FEM analysis of a four-point bending test sample. Moreover, the mechanical properties for this phase of our study derived from experimental data established in the first part of the study (see the Part I article).

By applying those experimental data to an FEM, we could compare different failure criteria (Tsai-Wu, Hoffmann, maximum stress) and establish that the Hoffman criterion was suitable for determining the rupture loads of those complex composites built with elastoviscoplastic materials (the mean difference between the results from the modeling and those from experimental data was 13.3%).

Finally, focusing on the object of this study, cylindrical LVL, we could determine the influence of the butt joint gap on the mechanical properties during bending. We showed that a critical size of the gap exists, under which both MOE and MOR increase suddenly of a non negligible amount (+9% in the case of the MOE, +52.5% in the case of the MOR), any other parameters remaining equal.

Acknowledgments The authors thank the Japanese Society for the Promotion of Science, which has supported this study, and the related work.

References

1. Yamauchi H, Shoho S, Yang P, Kawai S, Sasaki H (1997) Manufacturing of cylindrical LVL by spiral-winding method. I. Effect of interlocked-plies on the tensile Young's modulus. Mokuzai Gakkaishi 43:747–753
2. Yamauchi H, Miura I, Sasaki T, Koizumi A, Kawai S, Sasaki H (1998) Manufacturing condition and mechanical properties of cylindrical LVL manufactured by spiral-winding method (in Japanese). J Soc Mater Sci 47:350–355
3. Yang P, Ohsako Y, Yamauchi H, Sasaki H (1999) Numerical analysis of stress distribution along the glueline between cylindrical LVL column and its reinforcement core for end-joints. In: Proceedings the Pacific timber engineering conference, Rotorua, New Zealand
4. Yang P, Jinno K, Nishimoto A, Ohsako Y, Yamauchi H, Sasaki H (1999) Improving the bondability of injection-molded waste paper polyethylene composite. In: Proceedings of the 4th international conference on ecomaterials, Gifu, Japan
5. Yamauchi H, Kataya M, Ma L, Yamauchi S, Sasaki H (2002) Manufacturing of cylindrical LVL by spiral-winding method. IV. New method of isocyanate resin application using roll paper. Mokuzai Gakkaishi 48:432–438
6. Yamauchi H, Miura I, Okazaki Y, Kawai S, Sasaki H (2002) Manufacturing of cylindrical LVL by spiral-winding method. III. Relationships between tensile strength, veneer grain angle, and butt joint interval in LVL. Mokuzai Gakkaishi 48:363–370
7. Hata T, Umemura K, Yamauchi. H, Nakayama A, Kawai S, Sasaki H (2001) Design and pilot production of a "spiral-winder" for the manufacture of cylindrical laminated veneer lumber. J Wood Sci 47:115–123
8. Inaba D, Morita M, Nakano H, Takenaka A, Kawai S (2003) Continuous manufacture of cylindrical laminated veneer lumber. Bull Wood Res Inst Kyoto Univ 90:19–20
9. Gürdal Z, Haftka RT, Hajela P (1999) Design and optimization of laminated composites materials. Wiley, New York
10. Association Francaise de Normalisation (2004) NF-EN-408: structural timber and glued laminated lumber. AFNOR, France